Parametric resonance voltage response of electrostatically actuated Micro-Electro-Mechanical Systems cantilever resonators

Dumitru I. Caruntu [a,*], Israel Martinez [a], Martin W. Knecht [b]

[a] University of Texas-Rio Grande Valley, Mechanical Engineering Department, Edinburg, TX 78539, USA
[b] South Texas College, Engineering Department McAllen, TX 78501, USA

ARTICLE INFO

ABSTRACT

This paper investigates the parametric resonance voltage response of nonlinear parametrically actuated Micro-Electro-Mechanical Systems (MEMS) cantilever resonators. A soft AC voltage of frequency near natural frequency is applied between the resonator and a parallel ground plate. This produces an electrostatic force that leads the structure into parametric resonance. The model consists of an Euler–Bernoulli thin cantilever under the actuation of electrostatic force to include fringe effect, and damping force. Two methods of investigation are used, namely the Method of Multiple Scales (MMS) and Reduced Order Model (ROM) method. ROM convergence of the voltage response and the limitation of MMS to small to moderate amplitudes with respect to the gap (gap-amplitudes) are reported. MMS predicts accurately both Hopf supercritical and supercritical bifurcation voltages. However, MMS overestimates the large gap-amplitudes of the resonator, and. misses completely or overestimates the saddle-node bifurcation occurring at large gap-amplitudes. ROM produces valid results for small and/or large gap-amplitudes for a sufficient number of terms (vibration modes). As the voltage is swept up at constant frequency, the resonator maintains zero amplitude until reaches the subcritical Hopf bifurcation voltage where it loses stability and jumps up to large gap-amplitudes, next the gap-amplitude decreases until it reaches the supercritical Hopf bifurcation point, and after that the gap-amplitude remains zero, for the voltage range considered in this work. As the voltage is swept down at constant frequency, the zero gap-amplitude of the resonator starts increasing continuously after reaching the supercritical Hopf bifurcation voltage until it reaches the saddle-node bifurcation voltage when a sudden jump to zero gap-amplitude occurs. Effects of frequency, damping and fringe parameters on the voltage response show that (1) the supercritical Hopf bifurcation is shifted to lower voltage values with the increase of any of the mentioned parameters, (2) the subcritical Hopf bifurcation is shifted to larger voltage values with the increase of damping, shifted to lower voltage values with the increase of the fringe parameter, and not significantly altered by the change in frequency, (3) the saddle-node bifurcation voltage decreases with the increase of frequency and damping, and decrease of fringe parameter, and (4) the saddle-node bifurcation gap-amplitude decreases with the increase of frequency and damping, and it is not significantly altered by the change of the fringe parameter.

© 2015 Elsevier Ltd. All rights reserved.

* Corresponding author. Tel.: +1 956 665 2079; fax: +1 956 665 3527.
  E-mail addresses: dumitru.caruntu@utrgv.edu, caruntud2@asme.org, dcaruntu@yahoo.com (D.I. Caruntu).

1. Introduction

Micro-Electro-Mechanical Systems (MEMS) received attention over the past two decades. Small in size, low in weight and energy consumption, these systems are highly durable. This makes them excellent candidates for applications such as filters [1,2], mass sensors [3,4], switches [5], and microscopy probes [6,7].

Among the types of MEMS actuation, including piezoelectric and electro-magnetic, the electrostatic actuation is preferred due to its simplicity and efficiency. It provides significant force that can be controlled through an electric supply which consumes little power [8]. The electric load is composed of a DC polarization voltage and an AC voltage; the beam is deflected by the DC component and then driven to vibrate by the AC harmonic load [9,10]. A phenomenon associated with electrostatic actuation is pull-in. This phenomenon occurs when the voltage exceeds a threshold value, and consists of large deflections and ultimately a collapse of the MEMS flexible structure such as a cantilever onto the rigid plate, causing the device to fail. Pull-in is a basic instability phenomenon considered in design [9,11–14]. Also electric measurements can be used to characterize electrostatically actuated MEMS. Based on electric admittance measurements, resonance frequencies and quality factors of MEMS can be characterized [15].

Nonlinearities play a major role in MEMS dynamics. Nonlinearities arise from sources such as electrostatic actuation, squeeze-film damping, large deformations (geometric nonlinearities), and intermolecular forces. The electrostatic force is nonlinear, and if the voltage generating the force includes an AC voltage component besides the DC component, then the force is also parametric since periodic coefficients are present in the expression of the force. Therefore a voltage with an AC component produces nonlinear parametric excitations. Damping is important in the design of MEMS since it constitutes a major factor of energy dissipation [16]. Intermolecular forces, namely Casimir and van der Waals [17], are significant for gaps between the flexible structure and ground plate of MEMS less than 1 μm and 50 nm, respectively. The stability of such systems, and the types of nonlinearities that occur are highly sensitive to parameters such as initial amplitude, excitation frequency and excitation voltage. For nonlinear systems, bifurcation points (points where a sudden change in stability occurs) are of particular importance for design and control.

Investigations regarding nonlinear dynamics of MEMS have been reported in the literature. Nonlinear dynamics of MEMS cantilevers under both parametric and forcing excitations has been investigated using a lumped system model [18]. Electrostatically actuated microbeam suspended between two conductive micro-plates and subjected to the same actuation voltage has been investigated using a variational iteration method [19]. The nonlinear governing differential equation of motion has been reduced to a Mathieu type equation using a Galerkin based reduced order model. It was shown that although the applied DC voltage is equal or greater than the pull-in value by applying an AC voltage and adjusting its frequency the microbeam can be stabilized. However, the fringe effect has been neglected and only stability analysis has been conducted (no frequency or voltage responses were reported). Nonlinear size-dependent behavior of electrically actuated MEMS resonator, excited by an AC voltage which is superimposed on a DC voltage, based on the modified couple stress theory has been reported [20]. A high-dimensional reduced order model of the continuous system and the pseudo-arc length continuation technique has been employed for investigating the nonlinear static and dynamic behavior of the system. The fringe effect has not been included. Only clamped-clamped MEMS resonators have been investigated. A model of large deflections [21] for pull-in analysis of electrostatically actuated beams has been reported in the literature. Nonlinearities in the system were geometric due to large deflections and electrostatic due to the actuation. Yet, only a static analysis of the system under DC voltage, and dynamic behavior of suddenly applied DC voltage of the system have been reported. The nonlinear dynamics of electrostatically actuated micro- and nano-cantilever resonators due to a soft AC voltage has been investigated, and amplitude–frequency responses of primary resonance [11,22,23], amplitude–frequency responses of parametric resonance [12,24,25], and amplitude–voltage response of primary resonance [26] have been reported. A review of electrostatic pull-in instability in MEMS/NEMS can be found in Ref. [27].

Various methods of investigation are used in the nonlinear dynamics of MEMS. These methods include the Method of Multiple Scales (MMS) [26], Reduced Order Model method (ROM) [22], Harmonic Balance method [18], variational iteration method [19], and an iterative method [28], in which all iterations are linear, for solving the nonlinear dynamical system.

This paper deals with electrostatically actuated MEMS cantilever resonators for sensing applications. The electrostatic actuation is due to a soft AC voltage of frequency near natural frequency of the resonator. Soft AC is the voltage that produces soft electrostatic forces in the system, i.e. it produces small to very small amplitudes (with respect to the gap between the resonator and the ground plate) when the frequency is away from resonance zones. This actuation frequency leads the MEMS resonator into parametric resonance. The electrostatic force including the fringe effect is nonlinear while the damping is linear [11]. The equation of motion of the MEMS cantilever resonator is developed using the Euler–Bernoulli hypothesis of slender beams. The shear deformation and rotary inertia effects are neglected. Two methods, namely MMS and ROM, are used to solve the differential equation of motion describing the system. From two- to five-term ROMs are numerically solved using AUTO 07P, a software package for continuation and bifurcation problems. The steady-state solutions [29] of the voltage–amplitude response are determined.

To the best of our knowledge, this is the first time when it is reported (1) the voltage response of parametric resonance of electrostatically actuated MEMS cantilever (a distributed-parameter model) to include fringe effect and under a soft AC voltage actuation, (2) using two methods of investigation, namely MMS and ROM, in which (3) a convergence investigation of the ROM is conducted. (4) A good agreement between MMS and ROM is shown for gap-amplitudes (amplitudes with respect to the gap) less than 0.4. For large gap-amplitudes, up to pull-in (contact between the resonator and the ground
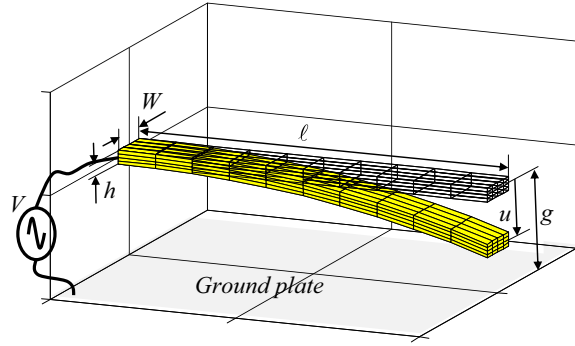
Fig. 1. Uniform MEMS resonator.

plate), (5) only five terms (vibration modes) ROM can accurately predict the behavior of the resonator; MMS fails in this range. (6) The effects of frequency, damping, and fringe effect on the voltage response are reported.

2. Dimensionless equation

Fig. 1 shows a deformable MEMS cantilever resonator over a parallel ground plate under electrostatic actuation. AC voltage between the ground plate and the MEMS cantilever generates an electrostatic force that leads to transverse vibrations of the cantilever. The dimensionless boundary value problem describing the motion of electrostatically actuated MEMS uniform cantilever resonators [11,12,23–26] is given by

$$
\begin{cases}
\dfrac{\partial^2 u(\tau,z)}{\partial \tau^2} + \dfrac{\partial^4 u(\tau,z)}{\partial z^4} = -b^* \dfrac{\partial u(\tau,z)}{\partial \tau} + \delta \cdot V^2(\tau) \left\{ \dfrac{1}{[1-u(\tau,z)]^2} + \dfrac{f}{[1-u(\tau,z)]} \right\} \\
u(\tau,0) = \dfrac{\partial u}{\partial z}(\tau,0) = \dfrac{\partial^2 u}{\partial z^2}(\tau,1) = \dfrac{\partial^3 u}{\partial z^3}(\tau,1) = 0
\end{cases}
\tag{1}
$$

Euler–Bernoulli theory is used. The shear and rotary inertia are neglected. The right hand side of Eq. (1) consists of three dimensionless forces, namely damping, electrostatic, and electrostatic due to fringe effect, in this order. The dimensionless variables of Eq. (1) are

$$
u = w/g; \quad z = x/\ell; \quad \tau = \frac{1}{\ell^2} \sqrt{\frac{EI_0}{\rho A_0}} \cdot t
\tag{2}
$$

where u, z and τ are dimensionless beam deflection, dimensionless longitudinal coordinate, and dimensionless time, respectively, and w, x, and t their corresponding dimensional variables. Also ℓ is cantilever length, g gap between cantilever and ground plate, E Young modulus, and ρ density. A_0 and I_0 are reference dimensional cross-section area and reference cross-section moment of inertia, respectively. While for uniform cantilevers they are the cross-section area and moment of inertia of the cantilever, for nonuniform cantilevers the reference cross-section could be where the cross-section area is maximum. Natural frequencies and mode shapes for such nonuniform structures have been reported in the literature [30–34]. In this work uniform cantilevers are investigated. The dimensionless parameters in Eq. (1) are given by

$$
b^* = \frac{b}{g}\sqrt{\frac{\ell^4}{\rho A_0 EI_0}}, \qquad \delta = \frac{\varepsilon_0 W \ell^4}{2g^3 EI_0} V_0^2, \qquad f = \frac{0.65g}{W}, \qquad \Omega^* = \Omega l^2 \sqrt{\frac{\rho A_0}{EI_0}}
\tag{3}
$$

where b^* is the dimensionless damping parameter, δ is the dimensionless voltage parameter, i.e. dimensionless amplitude of the electrostatic excitation force, f is the dimensionless fringe parameter, i.e. the parameter associated with a fringing correction to the electrostatic force, Ω^* the dimensionless frequency of excitation, V_0 dimensional amplitude of the AC voltage, b dimensional coefficient of viscous damping per unit length, W beam width, and $\varepsilon_0 = 8.854 \times 10^{-12}$ C^2 N^{-1} m^{-2} permittivity of free space. The viscous damping force is used, it is assumed that the resonator will operate in a viscous pressure regime [11]. The dimensionless voltage $V(\tau)$ in this investigation is considered as follows

$$
V(\tau) = \cos \Omega^* \tau
\tag{4}
$$

3. Parametric resonance $\Omega^* \approx \omega_k$

Parametric resonance, i.e. the the case of AC frequency near natural frequency of the MEMS resonator, $\Omega^* \approx \omega_k$, is investigated. The nearness of the excitation frequency can be written as

$$\Omega^* = \omega_k + \varepsilon\sigma \tag{5}$$

where σ is a detuning parameter, and ε is a dimensionless bookkeeping parameter used in MMS. The square of the voltage given by Eq. (4) can be written in terms of imaginary exponentials as

$$V^2(T_0) = \frac{1}{2} + \frac{1}{4}\left(e^{2\Omega^* i T_0} + e^{-2\Omega^* i T_0}\right) \tag{6}$$

One can notice that although the AC frequency is near natural frequency, the frequency of actuation of the electrostatic force is near twice the natural frequency, which results in parametric resonance.

4. Method of Multiple Scales

The Method of Multiple Scales (MMS) is an analytical approximate method which is valid for small nonlinearities and small amplitudes. Expanding out the last two terms of the right-hand side of Eq. (1) in Taylor series with $u = 0$ center and up to third-power in u, and considering small damping, and small electrostatic force and fringe effect, i.e parameters b^*, δ, and f are small, then Eq. (1) can be written as

$$\frac{\partial^2 u}{\partial \tau^2} + \frac{\partial^4 u}{\partial z^4} = -\varepsilon b^* \frac{\partial u}{\partial \tau} + 2\varepsilon\delta\, V^2(\tau) \sum_{n=0}^{3} C_{n+1} u^n, \quad C_n = \tfrac{1}{2}(n+f) \tag{7}$$

where ε is a small dimensionless bookkeeping parameter. A first-order expansion of the dimensionless transverse deflection u is then considered as follows:

$$u(z, \tau, \varepsilon) = u_0(z, T_0, T_1) + \varepsilon \cdot u_1(z, T_0, T_1) \tag{8}$$

where $T_0 = \tau$ is the fast time scale and $T_1 = \varepsilon\tau$ is the slow time scale, and the time derivative are given by $\partial/\partial\tau = D_0 + \varepsilon D_1$, where $D_0 = \partial/\partial T_0$, $D_1 = \partial/\partial T_1$ are the partial derivatives with respect to the slow and fast time scales. Replacing Eq. (8) and time derivatives into Eq. (7) and equating coefficients of like powers of ε, the following two approximation problems, zero-order and first-order, respectively, result as follows:

$$\text{Order } \varepsilon^0 \quad \begin{cases} D_0^2 u_0 + \frac{\partial^4 u_0}{\partial z^4} = 0 \\ Boundary \quad conditions \end{cases}, \tag{9}$$

$$\text{Order } \varepsilon^1 \quad \begin{cases} D_0^2 u_1 + \frac{\partial^4 u_1}{\partial z^4} = -2D_0 D_1 u_0 - b^* D_0 u_0 + 2\varepsilon\delta\, V^2(T_0) \sum_{n=0}^{3} C_{n+1} u_0^n \\ Boundary \quad conditions \end{cases} \tag{10}$$

The zero-order value boundary problem given by Eq. (9) is considered for the case of a cantilever MEMS resonator. The solution of the zero-order value boundary problem is given by

$$u_0(z, T_0, T_1) = \phi(z)\left[A(T_1)e^{i\omega T_0} + \overline{A}(T_1)e^{-i\omega T_0}\right] \tag{11}$$

where A and $\overline{A}$ are complex conjugate coefficients depending only on the slow time scale T_1. Imposing the cantilever boundary conditions on Eq. (11), the natural frequencies ω_k and their corresponding mode shapes $\phi_k(z)$ are obtained [11,12,23–26]. The mode shapes $\phi_k(z)$ form an othonormal set $\langle \phi_m, \phi_n \rangle = \int_0^1 \phi_m \phi_n dz = \delta_{mn}$ where δ_{mn} is Kronecker's delta.

The first-order approximation can be found by solving the inhomogeneous Eq. (10). Replacing Eq. (11) into Eq. (10), it results

$$D_0^2 u_1 + \frac{\partial^4 u_1}{\partial z^4} = -2D_0 D_1 \varphi_k\left[A_k(T_1)e^{i\omega_k T_0} + \overline{A_k}(T_1)e^{-i\omega_k T_0}\right] - b^* D_0 \varphi_k\left[A_k(T_1)e^{i\omega_k T_0} + \overline{A_k}(T_1)e^{-i\omega_k T_0}\right]$$

$$+ 2\delta V^2(T_0) \sum_{n=0}^{3} C_{n+1}\left[A_k(T_1)e^{i\omega_k T_0} + \overline{A_k}(T_1)e^{-i\omega_k T_0}\right]^n \tag{12}$$

After substituting Eqs. (5) and (6) into Eq. (12), the secular terms are collected and set equal to zero. The inhomogeneous Eq. (12) has a solution only if the solvability condition holds, i.e. the right-hand side is orthogonal to every solution of the homogenous problem, Eq. (9). Therefore it results

$$-2i\omega_k g_{1kk} A_k' - i\omega_k b^* g_{1kk} A_k + C_2\delta g_{1kk} A_k + 3C_4\delta g_{3kk} A_k^2 \overline{A}_k$$

$$+ \tfrac{1}{2}C_2\delta g_{1kk}\overline{A}_k e^{2i\sigma T_1} + \tfrac{3}{2}C_4\delta g_{3kk} A_k \overline{A}_k^2 e^{2i\sigma T_1} + \tfrac{1}{2}C_4\delta g_{3kk} A_k^3 e^{-2i\sigma T_1} = 0 \tag{13}$$

where A_k' is the derivative of A_k with respect to the slow time scale T_1. The coefficients g_{nkk} are given by

$$g_{nkk} = \langle \phi_k^n, \phi_k \rangle = \int_0^1 \phi_k^n \phi_k dz \tag{14}$$

where n is an integer greater than or equal to zero. A_k is expressed in polar form as follows

$$A_k = \frac{1}{2} a_k e^{i\beta_k}, \tag{15}$$

where a_k and β_k are real amplitude and real phase of the MEMS resonator, respectively. Substituting Eq. (15) into Eq. (13), separating the real and imaginary parts, and setting these parts equal to zero, the amplitude and phase slow scale differential equations result as

$$a_k' = a_k \left\{ -\frac{b^*}{2} + \left[C_2\delta + \frac{C_4\delta g_{3kk}}{2 g_{1kk}} a_k^2 \right] \frac{\sin 2\gamma_k}{4\omega_k} \right\} \tag{16}$$

$$a_k\gamma_k' = a_k\sigma + \frac{C_2\delta}{2\omega_k}a_k + \frac{3C_4\delta g_{3kk}}{8\omega_k g_{1kk}}a_k^3 + a_k \left[C_2\delta + C_4\delta \frac{g_{3kk}}{g_{1kk}}a_k^2 \right] \frac{\cos 2\gamma_k}{4\omega_k} \tag{17}$$

where γ_k is given by

$$\gamma_k = \sigma T_1 - \beta_k \tag{18}$$

The steady-state solutions result by substituting $a_k' = \gamma_k' = 0$ and voltage parameter into Eqs. (16) and (17). The trivial solution, $a_k = 0$, is a solution for all values of the detuning parameter σ and voltage parameter δ, as one can see from Eqs. (16) and (17). In addition, the non-trivial steady-state solutions are given by a set of parametric equations describing the response of resonator's amplitude a_k, phase γ_k, frequency σ, and voltage δ as

$$a_k^2 = \frac{2g_{1kk}}{C_4\delta g_{3kk}} \left(\frac{2\omega_k b^*}{\sin 2\gamma_k} - C_2\delta \right) \tag{19}$$

$$\sigma = -\frac{C_2\delta}{2\omega_k} - \frac{3C_4\delta g_{3kk}}{8\omega_k g_{1kk}}a_k^2 - \left[C_2\delta + C_4\delta \frac{g_{3kk}}{g_{1kk}}a_k^2 \right] \frac{\cos 2\gamma_k}{4\omega_k} \tag{20}$$

5. Reduced Order Model (ROM) of uniform MEMS resonators

A set of non-explicit ordinary differential equations to model the frequency response of the MEMS resonator using the Reduced Order Model (ROM) method is developed. Classified as ROM domain method, this method by "employing the mode shapes of the device can capture qualitative and quantitative changes in the device behavior and has a better performance in the presence of nonlinearities provided that enough modes are retained in the approximation" [35]. In what follows a ROM solution employing the resonator mode shapes is assumed as follows:

$$u(z, \tau) = \sum_{i=1}^N u_i(\tau)\varphi_i(z) \tag{21}$$

where N is the number of terms in the ROM, $u_i(\tau)$ and $\varphi_i(z)$ are the first N time dependent functions to be determined, and the linear undamped mode shapes of the uniform cantilever beam [11, 12, 23–26] which are given by

$$\varphi_k(z) = -\left\{ \cos\left(\sqrt{\omega_k}z\right) - \cosh\left(\sqrt{\omega_k}z\right) + C_k\left[\sin\left(\sqrt{\omega_k}z\right) - \sinh\left(\sqrt{\omega_k}z\right) \right] \right\} \tag{22}$$

where k is any nonzero positive integer, and ω_k are the corresponding natural frequencies. Afterwards, through a convergence process, the number of modes retained in the approximation is to be determined. The first five natural frequencies ω_k and coefficients C_k from Eq. (22) are given in Table 1. Eq. (1) is multiplied by $[1 - u(\tau, z)]^2$ in order to eliminate any displacement $u(z, \tau)$ from appearing in the denominator [11,12,23–26]. Then Eq. (21) is substituted into the resulting equation. The following relationships are satisfied by the mode shapes of the cantilever

$$u^{(4)} = \sum_{i=1}^N u_i\varphi_i^{(4)} = \sum_{i=1}^N \omega_i^2 u_i\varphi_i \tag{23}$$

Table 1
First five natural frequencies and mode shape coefficients of uniform. cantilever.

	$k=1$	$k=2$	$k=3$	$k=4$	$k=5$
ω_k	3.51562	22.0336	61.70102	120.91202	199.85929
C_k	−0.734	−1.0185	−0.9992	−1.00003	−1.00000

Therefore the resulting equation is given by

$$\sum_i^N \ddot{u}_i\varphi_i - 2\sum_{ij}^N \ddot{u}_i u_j\varphi_i\varphi_j + \sum_{ijk}^N \ddot{u}_i u_j u_k\varphi_i\varphi_j\varphi_k + b^*\sum_i^N \dot{u}_i\varphi_i - 2b^*\sum_{ij}^N \dot{u}_i u_j\varphi_i\varphi_j + b^*\sum_{ijk}^N \dot{u}_i u_j u_k\varphi_i\varphi_j\varphi_k$$

$$+ \sum_i^N \omega_i^2 u_i\varphi_i - 2\sum_{ij}^N \omega_i^2 u_i u_j\varphi_i\varphi_j + \sum_{ijk}^N \omega_i^2 u_i u_j u_k\varphi_i\varphi_j\varphi_k = \delta V^2(\tau) + f\delta V^2(\tau) - f\delta V^2(\tau)\sum_i^N u_i\varphi_i \tag{24}$$

Next, Eq. (24) is multiplied by mode shape $\varphi_n(z)$, and the entire equation is integrated from $z=0$ to $z=1$, where $n=1,2,...N$, and the orthonormality of the mode shapes $\varphi_i(z)$ is as

$$\int_0^1 \varphi_i\varphi_j dz = \delta_{ij} = \begin{cases} 0, i \neq j \\ 1, i = j \end{cases} \tag{25}$$

Depending on the number of terms used, this process leads to a ROM system of n second order coupled differential equations in time as follows

$$\ddot{u}_n - 2\sum_{ij}^N \ddot{u}_i u_j h_{nij} + \sum_{ijk}^N \ddot{u}_i u_j u_k h_{nijk} + b^*\dot{u}_n - 2b^*\sum_{ij}^N \dot{u}_i u_j h_{nij} + b^*\sum_{ijk}^N \dot{u}_i u_j u_k h_{nijk}$$

$$+ \omega_n^2 u_n - 2\sum_{ij}^N \omega_i^2 u_i u_j h_{nij} + \sum_{ijk}^N \omega_i^2 u_i u_j u_k h_{nijk} = (1+f)\delta V^2(\tau)h_n - f\delta V^2(\tau)u_n \tag{26}$$

where $n=1,2,...N$, V is given by Eqs. (4) and (5) for $\varepsilon = 1$, and

$$h_n = \int_0^1 \varphi_n dz, \quad h_{nij} = \int_0^1 \varphi_i\varphi_j\varphi_n dz, \quad h_{nijk} = \int_0^1 \varphi_i\varphi_j\varphi_k\varphi_n dz \tag{27}$$

6. Numerical results

The ROM system of n second order equations given by Eq. (26) is then transformed into a system of $2n$ first order differential equations as follows

$$\begin{cases} \dot{y}(2k-1) = y(2k) \\ \dot{y}(2k) = \ddot{u}_k \end{cases}, \quad k=1,2,...,N \tag{28}$$

where the new variables y are given by

$$\begin{cases} y(2k-1) = u_k \\ y(2k) = \dot{u}_k \end{cases}, \quad k=1,2,...,N \tag{29}$$

The second order derivatives $\ddot{u}_k$ from Eq. (28) are given by Eq. (26). The system of differential equations given by Eq. (28) is then integrated for four cases $N=2$, $N=3$, $N=4$, and $N=5$ using AUTO 07P, a software package for continuation and bifurcation problems [29] providing the steady-state solutions, both stable and unstable. In AUTO the computation of periodic solutions to a periodically forced system can be done by adding a nonlinear oscillator with the desired periodic forcing as one of the solution components. The voltage–amplitude response of the system near natural frequency has been investigated using a ROM from two to five terms ROM. Numerical simulations of this work have been conducted for MEMS cantilevers of dimensional characteristics given in Table 2 (and consequently dimensionless parameters given in Table 3).

Table 2
Dimensional system parameters.

Parameter	Symbol	Value
Beam width	W	20 μm
Beam length	ℓ	300 μm
Beam thickness	h	2.0 μm
Initial gap distance	g	8.0 μm
Material density	ρ	2330 kg/m^3
Young's modulus	E	169 GPa
Quality factor	Q	350
Peak AC voltage	V_0	12.5 V

Table 3
Dimensionless system parameters.

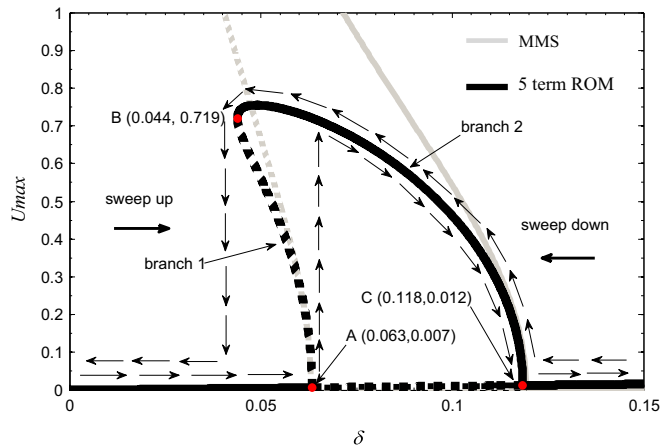| Damping	b^*	0.01
Amplitude of excitation (voltage)	δ	0.10
Fringe correction	f	0.26

Fig. 2. Amplitude–voltage response, parametric resonance, using MMS and five terms ROM. b^*=0.01, σ= −0.011 and f=0.26.

7. Discussion and conclusions

MEMS cantilever resonators are modeled as Euler–Bernoulli thin beams. No nonlinearities arise from the structure itself. The AC frequency is near natural frequency generating an electrostatic force (to include first-order fringe correction) that leads to parametric nonlinear resonance of the MEMS resonator. Parametric coefficients are found in both linear and nonlinear terms within the governing equation.

The dimensionless amplitude, namely the amplitude with respect to the gap given by Eq. (2), is called gap-amplitude. Although gap-amplitudes between 0.5 and 1 are referred to as large amplitudes (with respect to the gap), the amplitudes of the MEMS cantilever resonator are small to moderate due to its slenderness ratio $s = \ell \sqrt{A_0/I_0}$ larger than 100, and small gap compared to its length. The gap-amplitude is referred to as amplitude or dimensionless amplitude.

Two methods, namely MMS and ROM, are used to investigate the behavior of the system. ROM is able to accurately capture the behavior of the system for moderately large deflections up to the pull-in instability limit, while MMS which is a perturbation method could not [9,11,21,23–26,36]. Using five modes (five terms) ROM guarantees the convergence of the steady state amplitude [9,11,21,23–26,36]. Figs. 2–6 show a comparison between MMS and ROM, ROM convergence, effect of dimensionless damping on the voltage response of the MEMS resonator, effect dimensionless voltage parameter, and effect of the dimensionless fringe parameter, respectively.

The ROM is more accurate for larger deflections. The increased accuracy comes at a cost, though. First the ROM is more costly in the form of computational time. Five term ROM in Fig. 2 takes 126 s of computational time on a Dell Desktop, Intel (R) Core(TM) 2 Duo CPU @ 2.33 GHz, with 8 GB RAM, and a 64-bit operating system, whereas the MMS plot in the same Fig. 2 was plotted in less than 2 s. The MMS is computationally more efficient than methods using direct numerical integration such as ROM. Second, numerical methods such as the ROM have an underlying problem of not providing an insight into the underlying physics and interactions of a system [11]. An analytical approach, such as the MMS, can allow for a faster insight regarding the types of resonances as well as effects of various parameters on the responses of the system.

Fig. 2 shows the steady-state solutions of the voltage response of the parametric resonance of the MEMS resonator. A comparison between two methods, MMS (gray lines) and 5 terms ROM (black lines) is illustrated. In the horizontal axis is the dimensionless voltage δ and in the vertical axis is the dimensionless amplitude of the tip of the cantilever $Umax$. Solid line branches represent stable solutions, and dash line branches unstable solutions. Next, the ROM prediction of the resonator's behavior is discussed. One can see that zero amplitude steady-states are solutions of the voltage response, for all values of δ considered, and that these solutions are stable except between the bifurcation points A and C. Points A and C are subcritical and supercritical Hopf bifurcation points, respectively. As the voltage is swept up the amplitude stays zero until it reaches the bifurcation point A. At this point the steady-state solution becomes unstable and a sudden jump from point A to the corresponding point (same voltage) on the branch BC occurs. This is a sudden change in amplitude from zero to 0.7 of the gap. As the voltage continues to be swept up the amplitude decreases along branch BC until it reaches at the bifurcation
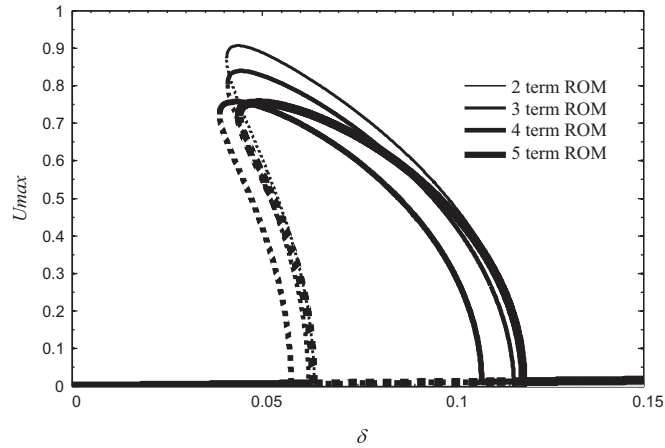
Fig. 3. Amplitude–voltage response, parametric resonance, using two, three, four, and five terms ROM. $b^*=0.01$, $\sigma=-0.011$ and $f=0.26$.
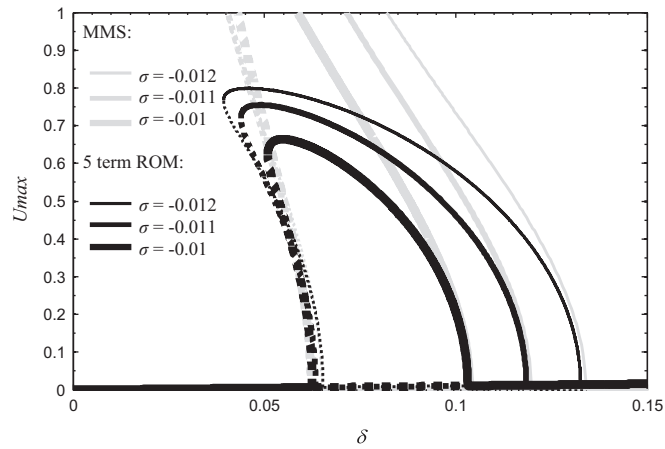

Fig. 4. Effect of the dimensionless frequency parameter σ using MMS and five terms ROM. $b^*=0.01$ and $f=0.26$.
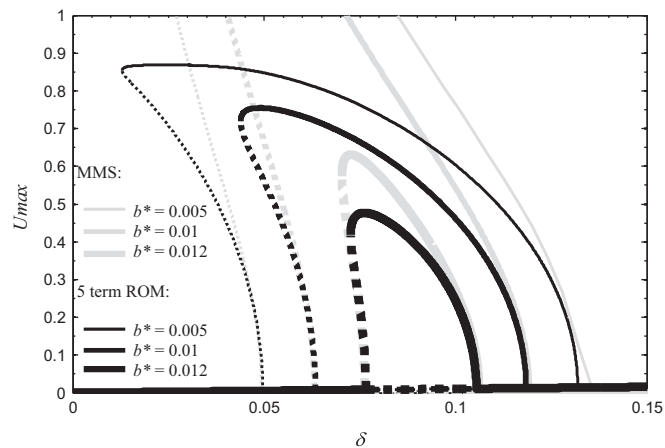

Fig. 5. Effect of the dimensionless damping parameter b^* using MMS and five term ROM. $\sigma=-0.011$ and $f=0.26$.

point C the value of zero. The amplitude will stay zero for any further increase of the voltage up to $\delta=0.15$. This is illustrated by the arrows from the origin to A, up to the branch BC, along this branch to point C, and then on the δ-axis to the right-hand side. As the voltage is swept down from $\delta=0.15$, the amplitude stays zero until it reaches the bifurcation point C. Then the amplitude increases along branch BC until it reaches the saddle-node bifurcation point B. Here the steady-state amplitude becomes unstable and jumps down to zero amplitude (on δ-axis) and continues to remain zero until the voltage is swept
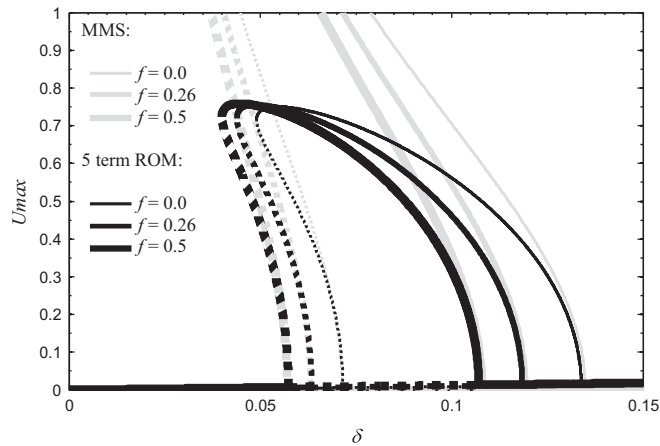
Fig. 6. Effect of the fringe correction f using MMS and a five terms ROM. $\sigma = -0.011$ and $b^* = 0.01$.

down to zero. This behavior is illustrated by the arrows from $\delta = 0.15$ to the left-hand side to bifurcation point C, along BC branch up to point B, down to δ–axis, and to the origin along δ–axis.

The two methods MMS and 5T ROM show a perfect agreement for amplitudes less than 0.4 of the gap. However, they predict total different behaviors for large amplitudes. MMS which is an asymptotic, perturbation method, is valid for weak nonlinearities and relatively small amplitudes. Consequently, MMS predictions are not reliable for amplitudes larger than 0.5 of the gap. MMS fails to predict the behavior in this range of amplitudes. MMS does not predict the bifurcation point B. However, MMS is an approximate analytical method extremely useful for finding the bifurcation points A and C. Conversely ROM is a method that that is valid not only for systems with weak nonlinearities and small amplitudes, but also for systems with strong nonlinearities and large amplitudes. Therefore ROM is a reliable method for any range of nonlinearities and amplitudes provided a sufficient number of terms are considered.

Fig. 3 shows the convergence of the ROM method on the voltage–amplitude response. The convergence is showed by increasing the number of terms, $N = 2, 3, 4$ and 5, in the ROM. Numerical simulations conducted in this research demonstrate that five terms are required to accurately predict the behavior of the system for large amplitudes.

Fig. 4 illustrates the effect of the detuning frequency σ on the voltage–amplitude response. As frequency increases (1) Hopf bifurcation points A and C are shifted to lower voltage values, bifurcation point C more than bifurcation point A, (2) Conversely, bifurcation point B is shifted to larger voltage values, while its amplitude decreases. (3) The voltage interval AC, for which nonzero steady-state amplitudes are reached, decreases. (4) The amplitude peak decreases as well as. One can conclude that an increase in frequency narrows the voltage interval (with the lower end of the interval not significantly changing) and decreases the peak values of the nonzero steady-states amplitudes.

Fig. 5 shows the effect of damping b^* on the voltage–amplitude response, which is similar to some extent to the effect of increasing the frequency, Fig. 4. While increasing damping (1) bifurcation point C shifts to lower voltage values, and (2) bifurcation point B to higher voltage values, and (3) the peak amplitude decreases. This is the similarity. What is different is (4) the significant shift of the bifurcation point A to higher voltage values. One can conclude that the increase in damping reduces the nonlinear effect and the peak amplitude, and narrows (almost symmetrically) the voltage interval AC of nonzero steady-state amplitudes.

Fig. 6 illustrates the effect of fringe correction f on the voltage–amplitude response. The increase of the fringe effect f shifts (1) all bifurcation points A, B, and C to lower voltage values, C more significantly than A and B, but does not significantly affect the peak amplitude of the voltage–amplitude response. One can conclude that increasing the fringe effect (narrower beams) reduces the voltage interval AC of nonzero steady-state amplitudes to some extent, and significantly shifts the interval to lower voltage values while the peak amplitude of the response is not affected.

1. The limitations of this paper are as follows. This work is valid for (1) Euler–Bernoulli beams (slender beams), i.e. beams of slenderness ratio $s = \ell \sqrt{A_0 / I_0}$ larger than 100. It has been reported in the literature that "when the slenderness ratio is larger than hundred ($s > 100$) the Euler–Bernoulli model should be used, and when the slenderness ratio is small, either shear or Timoshenko model can be used" [37]. If the slenderness is "relatively large and only a few modes are significant in a solution, then the difference between solutions for the two models," Euler–Bernoulli and Timoshenko, "is too small to be of practical importance." [38]. For slender beams, the first five dimensionless natural frequencies of cantilevers have values of no significant difference regardless what theory one uses, namely Euler–Bernoulli, Rayleigh or Timoshenko [39]. Also Refs. [40,41] report comparisons of various theories regarding the first five natural frequencies of simply supported beams. Other comparisons between linear beam theories can be found in Refs. [42–44].
2. This work is valid for small to moderate amplitudes of MEMS cantilever resonators. Although, the gap-amplitude (amplitude with respect to the gap) is discussed to be small and/or large in this work, the amplitudes of the cantilever are

in the range of small to moderate due to the large length of the cantilever compared to its thickness and the gap. The MEMS resonators have relatively small slopes. This work is not valid for large amplitudes, when geometrical nonlinearities cannot be neglected.

3. The results of this paper are valid for "MEMS cantilevers of width to thickness ratio greater than five, and gap to thickness ratio greater than two," [23,26,45] "since Palmer formula for electrostatic force is used" [24].

Acknowledgments

References

[1] J.F. Rhoads, S.W. Shaw, Tunable microelectomechanical filters that exploit parametric resonance, *Journal of Vibration and Acoustics* 127 (5) (2005) 423–430.
[2] M. Gurbuz, T.F. Parlak, A. Bozhurt Bechteler, Analytical design methodology for microelectromechanical (MEM) filters, *Sensors and Actuators A* 119 (2005) 38–47.
[3] W. Zhang, K.L. Turner, Application of parametric resonance amplification in a single-crystal silicon micro-oscillator based mass sensor, *Sensors and Actuators A* 122 (2005) 23–30.
[4] W. Zhang, R. Baskaran, K.L. Turner, Effect of cubic nonlinearity on auto-parametrically amplified resonant MEMS mass sensor, *Sensors and Actuators A* 102 (2002) 139–150.
[5] K. Vummidi, M. Khater, E.M. Abdel-Rahman, A.H. Nayfeh, S. Raman, Dynamic pull-in of shunt capacitive MEMS switches, *Procedia Chem.* 1 (2009) 622–625.
[6] H. Yabuno, H. Kaneko, Van der Pol type self-excited micro-cantilever probe of atomic force microscopy, *Nonlinear Dynamics* 54 (2008) 137–149.
[7] K.M. Cheng, Z. Weng, D.R. Oliver, D.J. Thomson, G.E. Bridges, Microelectromechanical resonator characterization using noncontact parametric electrostatic excitation and probing, *Journal of Microelectromechanical Systems* 16 (5) (2007) 1054–1060.
[8] J. Stulemeijer, J.A. Bielen, P.G. Steeneken, J. Bouwe van der Berg, Numerical path following as an analysis method for electrostatic MEMS, *Journal of Microelectromechanical Systems* 18 (2) (2009) 488–499.
[9] A.H. Nayfeh, M.I. Younis, E.M. Abdel-Rahman, Dynamic pull-in phenomenon in MEMS resonators, *Nonlinear Dynamics* 48 (1–2) (2007) 153–163.
[10] E.M. Abdel-Rahman, A.H. Nayfeh, M.I. Younis, Dynamics of an electrically actuated resonant microsensor, in: Proceedings of the International Conference on MEMS, NANO and Smart Systems, Banff, Canada, July 2003, pp.188-196.
[11] D.I. Caruntu, M.W. Knecht, On nonlinear response near half natural frequency of electrostatically actuated microresonators, *International Journal of Structural Stability and Dynamics* 11 (4) (2011) 641–672.
[12] D.I. Caruntu, K.N. Taylor, Bifurcation type change of AC electrostatically actuated MEMS resonators due to DC bias, *Shock and Vibration* 2014 (2014). Article ID 542023, 1–9.
[13] M.M. Zand, M.T. Ahmadian, B. Rashidian, Semi-analytic solutions to nonlinear vibrations of microbeams under suddenly applied voltages, *Journal of Sound and Vibration* 325 (1-2) (2009) 382–396.
[14] F.M. Alsaleem, M.I. Younis, H.M. Ouakad, On the nonlinear resonances and dynamic pull-in of electrostatically actuated resonators, *Journal of Micromechanics and Microengineering* 19 (4) (2009) 045013 1–14.
[15] S. Kalicinski, H.A.C. Tilmans, M. Wevers, I. De Wolf, A new characterization method for electrostatically actuated resonant MEMS: determination of the mechanical resonance frequency, quality factor and dielectric charging, *Sensors and Actuators A* 154 (2009) 304–315.
[16] M. Zamanian, S.E. Khadem, Analysis of thermoelastic damping in microresonators by considering the stretching effect, *International Journal of Mechanical Sciences* 52 (10) (2010) 1366–1375.
[17] A. Ramezani, A. Alasty, J. Akbari, Closed-form solutions of the pull-in instability in nano-cantilevers under electrostatic and intermolecular surface forces, *International Journal of Solids and Structures* 44 (14–15) (2007) 4925–4941.
[18] W. Zhang, G. Meng, Nonlinear dynamical system of micro-cantilever under combined parametric and forcing excitations in MEMS, *Sensors and Actuators A* 119 (2005) 291–299.
[19] G. Rezazadeh, H. Madinei, R. Shabani, Study of parametric oscillation of an electrostatically actuated microbeam using variational iteration method, *Applied Mathematical Modelling* 36 (2012) 430–443.
[20] M.H. Ghayesh, H. Farokhi, M. Amabili, Nonlinear behaviour of electrically actuated MEMS resonators, *International Journal of Engineering Science* 71 (2013) 137–155.
[21] S. Chaterjee, G. Pohit, A large deflection model for the pull-in analysis of electrostatically actuated microcantilever beams, *Journal of Sound and Vibration* 322 (4–5) (2009) 969–986.
[22] D.I. Caruntu, L. Luo, Frequency response of primary resonance of electrostatically actuated CNT cantilevers, *Nonlinear Dynamics* 78 (3) (2014) 1827–1837.
[23] D.I. Caruntu, I. Martinez, M.W. Knecht, ROM analysis of frequency response of AC near half natural frequency electrostatically actuated MEMS cantilevers, *Journal of Computational and Nonlinear Dynamics* 8 (1) (2013) 031011 1–6.
[24] D.I. Caruntu, I. Martinez, Reduced order model of parametric resonance of electrostatically actuated MEMS cantilever resonators, *International Journal of Non-Linear Mechanics* 66 (1) (2014) 28–32.
[25] D.I. Caruntu, M.W. Knecht, Micro-electro-mechanical systems cantilever resonators under soft AC voltage of frequency near natural frequency, *Journal of Dynamic Systems, Measurement and Control* 137 (2015) 041016 1–8, http://dx.doi.org/10.1115/1.4028887.
[26] D.I. Caruntu, I. Martinez, K.N. Taylor, Voltage-amplitude response of alternating current near half natural electrostatically actuated MEMS resonators, *Mechanics Research Communications* 52 (1) (2013) 25–31.
[27] W.-M. Zhang, H. Yan, Z.-K. Peng, G. Meng, Electrostatic pull-in instability in MEMS/NEMS: a review, *Sensors and Actuators A* 214 (2014) 187–218.
[28] Y.M. Chen, G. Meng, J.K. Liu, An iterative method for nonlinear dynamical system of an electrostatically actuated micro-cantilever, *Physics Letters A* 374 (2010) 3455–3459.
[29] E.J. Doedel, B.E. Oldeman, AUTO-07P: Continuation and bifurcation software for ordinary differential equations, Concordia University, Montréal, Canada, 2009.
[30] D.I. Caruntu, Classical Jacobi polynomials, closed-form solutions for transverse vibrations, *Journal of Sound and Vibration* 306 (3–5) (2007) 467–494.

[31] D.I. Caruntu, Dynamic modal characteristics of transverse vibrations of cantilevers of parabolic thickness, *Mechanics Research Communications* 33 (3) (2009) 391–404.
[32] D.I. Caruntu, Self-adjoint differential equations for classical orthogonal polynomials, *Journal of Computational and Applied Mathematics* 180 (1) (2005) 107–118.
[33] D.I. Caruntu, Factorization of self-adjoint ordinary differential equations, *Applied Mathematics and Computation* 219 (1) (2013) 7622–7631.
[34] D.I. Caruntu, Eigenvalue singular problem of factorized fourth-order self-adjoint differential equations, *Applied Mathematics and Computation* 224 (1) (2013) 603–610.
[35] A.H. Nayfeh, M.I. Younis, E.M. Abdel-Rahman, Reduced-order models for MEMS applications, *Nonlinear Dynamics* 41 (1-3) (2005) 211–236.
[36] M.I. Younis, E.M. Abdel-Rahman, A.H. Nayfeh, A reduced-order model for electrically actuated microbeam-based MEMS, *Journal of Microelectromechanical Systems* 12 (5) (2003) 672–680.
[37] S.M. Han, H. Benaroya, T. Wei, Dynamics of transversely vibrating beams using four engineering theories, *Journal of Sound and Vibration* 225 (5) (1999) 935–988.
[38] A. Labuschagne, N.F.J. van Rensburg, A.J. van der Merwe, Comparison of linear beam theories, *Mathematical and Computer Modelling* 49 (2009) 20–30.
[39] A. Plankis, M. Lebsack, P.R. Heyliger, Elasticity-based beam vibrations for various support conditions, Applied Mathematical Modelling http://dx.doi.org/10.1016/j.apm.2015.02.023.
[40] R.A. Jafari-Talookolaei, M.H. Kargarnovin, M.T. Ahmadian, M. Abedi, An investigation on the nonlinear free vibration analysis of beams with simply supported boundary conditions using four engineering theories, *Journal of Applied Mathematics* 2011 (2011). Article ID 842805 1–17.
[41] H. Darijani, H. Mohammadabadi, A new deformation beam theory for static and dynamic analysis of microbeams, *International Journal of Mechanical Sciences* 89 (2014) 31–39.
[42] N.F.J. van Rensburg, A.J. van der Merwe, Natural frequencies and modes of a Timoshenko beam, *Wave Motion* 44 (2006) 58–69.
[43] L. Majkut, Free and forced vibrations of Timoshenko beam by single difference equation, *Journal of Theoretical and Applied Mechanics* 47 (1) (2009) 193–210.
[44] L.G. Villanueva, R.B. Karabalin, M.H. Matheny, D. Chi, J.E. Sader, M.L. Roukes, Nonlinearity in nanomechanical cantilevers, *Physical Review B* 87 (2) . Article Number 024304. http://dx.doi.org/10.1103/PhysRevB.87.024304..
[45] R.C. Batra, M. Porfiri, D. Spinello, Electromechanical model of electrically actuated narrow beams, *Journal of Microelectromechanical Systems* 15 (2006) 1175–1189.